Lab Notes

Editors
Thomas M. Moses | Shane F. McClure
Sally Eaton-Magaña

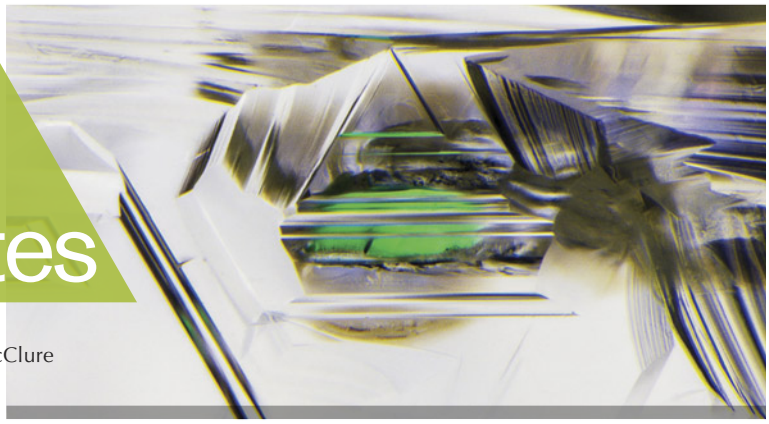

Star AQUAMARINE

The Carlsbad laboratory recently received a grayish blue aquamarine for an identification report. The unique 13.37 ct oval double cabochon displayed a six-rayed star (figure 1). Standard gemological testing revealed a spot refractive index of 1.570 and a hydrostatic specific gravity of 2.68. Raman analysis confirmed that the stone was beryl.

Under magnification (figure 2), the stone displayed planes of negative crystals, film-like inclusions, ilmenite, and reflective particles that resulted in a six-rayed star. Asterism in aquamarine is due to three sets of elongated channel-like or thin-film inclusions oriented in three different directions perpendicular to the *c*-axis (e.g., Spring 2004 Gem News International, p. 104; K. Schmetzer et al., "Asterism in beryl, aquamarine, and emerald—an update," *Journal of Gemmology*, Vol. 29, No. 2, 2004, pp. 66–71). Of all the aquamarines examined at GIA laboratories, this was one of the first to display asterism.

Jessa Rizzo

Figure 1. A 13.37 ct grayish blue aquamarine displaying asterism.

Rare Faceted BRUCITE

Gem-quality transparent blue brucite is a very rare, very soft and heat-sensitive magnesium hydroxide ($Mg(OH)_2$) with a Mohs hardness of approximately 2.5–3.0 and perfect cleavage. Brucite was named in 1824 in honor of the first person to describe the species: Archibald Bruce, an American mineralogist, physician, and editor of the *American Mineralogical Journal.*

Recently the Carlsbad laboratory received for identification services a transparent greenish blue stone weighing 3.09 ct and measuring 9.74 × 9.71 × 5.98 mm (figure 3). Microscopic observation revealed numerous scratches and abrasions on the surface, as well as strong doubling, some needles, and a large fracture. Standard gemological testing yielded a specific gravity of 2.37. Refractive index was not measured for fear of damaging this soft and fragile stone. A uniaxial optic character was observed with a polari-

Figure 2. Negative crystals, film-like inclusions, and ilmenite were observed under magnification in the star aquamarine. Field of view 3.57 mm.

Editors' note: All items were written by staff members of GIA laboratories.

Gems & Gemology, Vol. 59, No. 2, pp. 210–221.

Figure 3. A rare and very fragile 3.09 ct brucite.

scope and optic figure sphere. Raman spectroscopy confirmed the gem's identity as brucite. Worldwide, this was the second brucite examined by GIA.

Michaela Damba

DIAMOND

Natural Diamond with CVD-Like Fluorescence Pattern

Fluorescence images collected using the DiamondView are very useful in identifying whether a diamond is natural or laboratory grown (S. Eaton-Magaña and J.E. Shigley, "Observations on CVD-grown synthetic diamonds: A review," Fall 2016 *G&G*, pp. 222–245). In many cases, type II natural diamonds show varying dislocation networks in these images. Meanwhile, high-pressure, high-temperature (HPHT) synthetic diamonds show cuboctahedral growth patterns, and chemical vapor deposition (CVD) laboratory-grown diamonds show growth striations.

The Mumbai laboratory recently received a 0.40 ct colorless round brilliant for diamond grading service. Spectroscopy identified it as a type IIa diamond, and it was examined further for color origin determination. DiamondView imaging showed uncommon and interesting patterns. In figure 4, the lower right is dominated by green fluorescence while the upper left shows mainly blue fluorescence, with a clear and straight boundary. Detailed examination revealed numerous sharp and clear dislocation lines in multiple orientations in both parts of this diamond. These dislocation lines were introduced by plastic deformation and provide strong evidence that the diamond crystallized in nature. It should be pointed out that the interface layer seen in the fluorescence image is uncommon for natural diamonds but similar to that of CVD laboratory-grown diamonds. Further photoluminescence spectroscopy analysis confirmed this natural diamond was treated by annealing under high pressure and high temperature to improve its color, reinforcing our assertion that advanced analytical study is often crucial in identifying a diamond.

Natural grown diamonds with fluorescence patterns similar to those of HPHT synthetic diamonds have also been reported previously (Spring 2013 Lab Notes, pp. 45–46). With recent advances in technology, manufactured diamonds with unique features have become more widely available on the market. Therefore, it is more important than ever to scrutinize each feature to ensure the appropriate identification results in such scenarios. Since natural and manufactured diamonds are structurally identical, we often need to rely on advanced gemological and spectroscopic data, particularly for such low-nitrogen diamonds, to correctly identify their origin.

Manisha Bhoir and Shoko Odake

Yellow Zoning in Pink Diamonds

Recently GIA's Carlsbad laboratory received a few unusual natural, nitrogen-rich type IaA pink diamonds for color origin and identification service. The pink color of these diamonds is caused by the 550 nm visible absorption band, with the color concentrated within parallel narrow bands known as pink graining (S. Eaton-Magaña et al., "Natural-color pink, purple, red and brown diamonds: Band of many colors," Winter 2018 *G&G*, pp. 352–377). In diffused light, they displayed faint yellow color zoning (fig-

Figure 4. DiamondView imaging of the pavilion facets for this HPHT-treated natural diamond shows graining and zoning that resemble those of a laboratory-grown CVD diamond with HPHT treatment. The inset shows the DiamondView image of an HPHT-treated CVD-grown diamond.

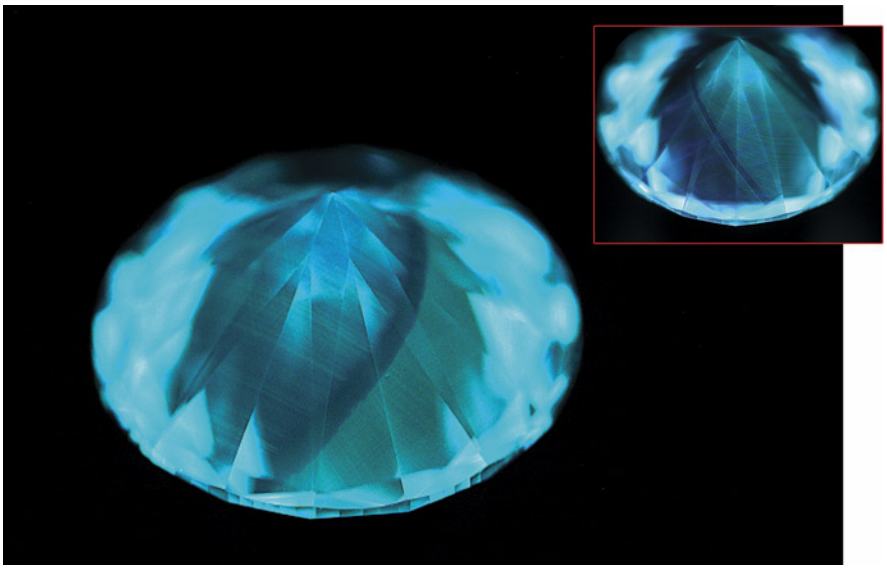

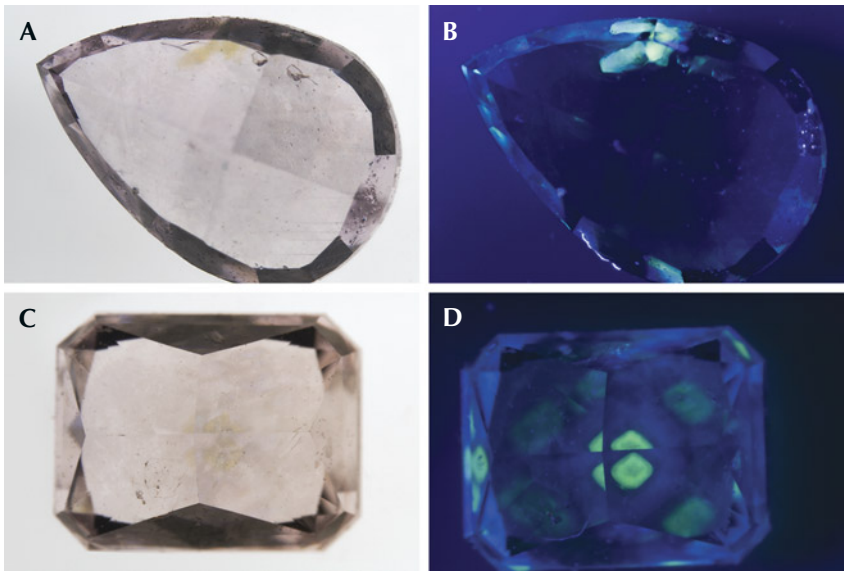

Figure 5. Fancy brownish pink pear and rectangular diamonds, each weighing 0.25 ct, shown in diffused light (A and C) and in long-wave UV light (B and D).

ure 5, A and C). Further inspection under long-wave UV revealed strong yellow fluorescence confined to areas with yellow color zoning (figure 5, B and D).

Photoluminescence (PL) spectra (excited by 514 nm laser) collected from the area with yellow zoning show a broad band centered at ~710 nm. This broad emission band and corresponding strong yellow fluorescence are typically observed in yellow or orange diamonds colored by the 480 nm visible absorption band (C.M. Breeding et al., "Naturally colored yellow and orange gem diamonds: The nitrogen factor," Summer 2020 *G&G*, pp. 194–219). These gemological and spectroscopic features suggest that separate color centers produce pink and yellow colors within these diamonds, though the 480 nm visible absorption band cannot be detected with ultraviolet/visible/near-infrared (UV-Vis-NIR) spectroscopy (possibly due to the fact that the yellow color zone is volumetrically small compared to the rest of the diamond, and that the UV-Vis-NIR absorption spectroscopy is a bulk analysis technique).

The mechanism of the formation of these unusual pink diamonds has not been determined and to the authors' knowledge, such diamonds showing localized regions colored by the 550 nm band and 480 nm band have not yet been documented. Since we know very little about the physics of the 480 and 550 nm visible absorption bands, their co-occurrence within single diamonds might help us to better understand the structures of defects that are related to these features. By paying careful attention to the details of color and fluorescence zoning, more of these unusual rare pink diamonds may be identified.

Shiva Sohrabi, Mei Yan Lai, and Sally Eaton-Magaña

GLASS Imitation of Cat's-Eye Chrysoberyl

The Hong Kong laboratory recently examined a ring mounted with an estimated 5.56 ct brownish yellow cat's-eye cabochon (figure 6). The client submitted the stone as cat's-eye chrysoberyl, which it resembled at first glance. Standard gemological testing yielded a spot refractive index of 1.57, well below chrysoberyl's range of 1.74–1.75. Under short-wave UV radiation, the stone displayed strong chalky fluorescence. Microscopic observation revealed long parallel tubes creating a cat's-eye when viewed from the top and a honeycomb structure when viewed from the side of the stone (figure 7). This confirmed the material was fiber-

Figure 6. A ring mounted with an estimated 5.56 ct brownish yellow cat's-eye cabochon resembling chrysoberyl.

Figure 7. The cabochon displayed the honeycomb structure frequently observed in fiber-optic glass. Field of view 2.00 mm.

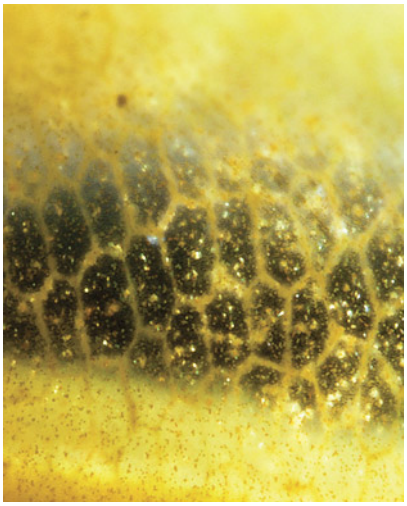

optic glass, made by fusing together very thinly spun glass fibers. Infrared spectroscopy showed two broad absorptions centered at 3500 and 2670 cm^{-1} associated with artificial glass, further validating our identification.

Artificial glass has been used as an imitation for different gems such as star sapphire (Fall 2021 Lab Notes, pp. 261–262), Paraíba tourmaline (Winter 2020 Lab Notes, pp. 518–520), nephrite and jadeite (Spring 2019 Lab Notes, pp. 93–94), and blue amber (Fall 2019 Gem News International, pp. 443–444). Its color and appearance can often lead to misidentification. Therefore, conducting basic gemological tests and observing the stone under a microscope is important, especially when the stone is set in jewelry.

Tsz Ying Fong

LABORATORY-GROWN DIAMOND

CVD Diamond Over 34 Carats

Chemical vapor deposition (CVD) growth technology has advanced significantly over the last two decades. In this study, we report on the largest CVD gem diamond GIA has encountered, recently tested in the Hong Kong laboratory. This emerald-cut diamond weighing 34.59 ct and measuring 24.94 × 13.95 × 9.39 mm (figure 8) was produced by Ethereal Green Diamond in India. It had G color and VS_2 clarity. Small black graphite inclusions were found. Some stood alone inside the body, while others formed clusters of clouds located between growth layers. Microscopic observation showed a weak oily or wavy graining when looking through the table facet, a feature sometimes seen in CVD gem diamonds. It tends to appear more prominently in CVD diamonds with high amounts of strain and a strong birefringence pattern when viewed through crossed polarizers (figure 9).

Infrared absorption spectroscopy revealed no absorption related to nitrogen, which is consistent with type IIa diamond. However, a weak absorption related to boron (an absorption peak at ~2800 cm^{-1}) was detected, corresponding to around 2 ppb of boron impurity. This trace amount of boron was very likely due to contamination during diamond growth. There are different opinions on whether this trace contamination should be considered in diamond type classification.

Photoluminescence (PL) spectroscopy was performed at liquid nitrogen temperature (–196°C) with several laser excitations (figure 10). In addition to strong emissions from NV^0 and NV^- centers at 575 nm and 637 nm, respectively, moderately strong doublet emissions from SiV^- at 736.6 and 736.9 nm were recorded. A weak emission at 946.4 nm, possibly from the SiV^0 defect, was also observed. Other important emission features included a strong emission from the H3 defect at 503.2 nm and a weak emission band with peaks at 566.0, 566.7, and 567.7 nm. The emission at 467.6 nm, which is common in as-grown CVD diamonds, was reduced by high-temperature treatment. These observations and spectroscopic features confirmed that this CVD diamond was annealed under high pressure and high temperature (HPHT) to improve its color appearance. In contrast, no post-growth color treatment was applied to the 16.41 ct CVD lab-grown diamond tested a year earlier in the New York laboratory (W. Wang et al., "New

Figure 8. This 34.59 ct CVD-grown diamond (24.94 × 13.95 × 9.39 mm), produced by Ethereal Green Diamond in India, is the largest GIA has tested.

Figure 9. A high amount of strain and a strong birefringence pattern were observed using crossed polarizers. Field of view 15.92 mm.

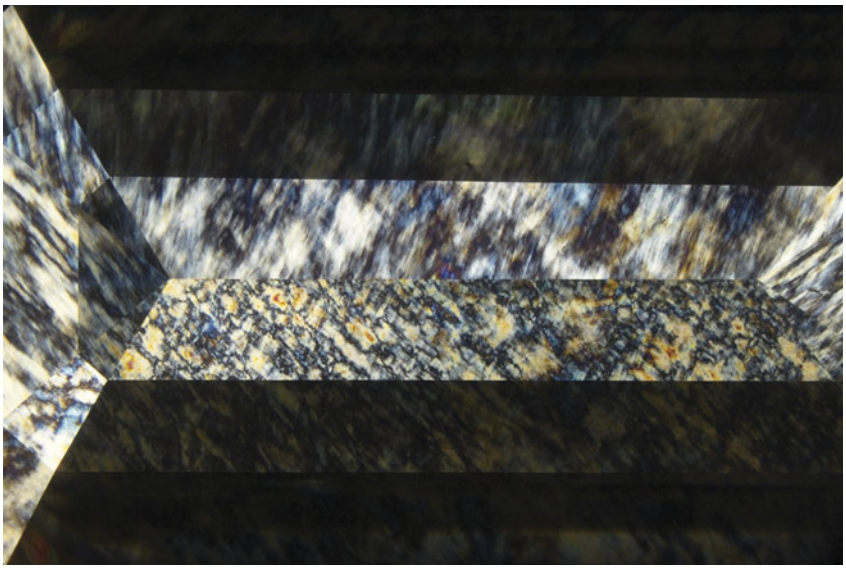

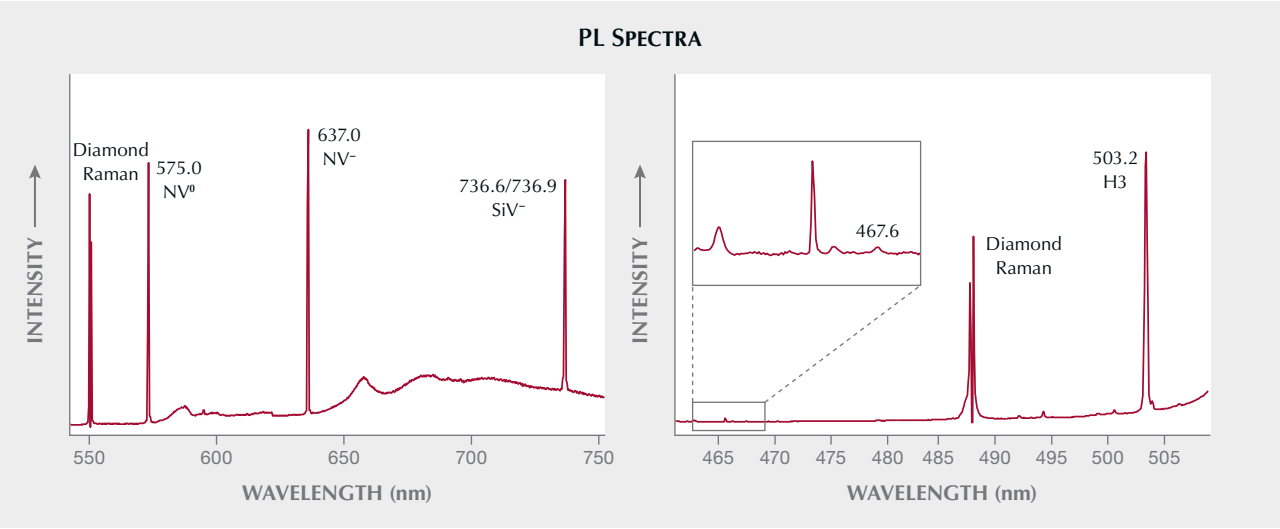

Figure 10. Left: The PL spectrum with 514 nm laser excitation under liquid nitrogen temperature showed features of treated CVD diamond. Right: The PL spectrum with 457 nm laser excitation under liquid nitrogen temperature recorded a strong H3 defect and a negligible 467.6 nm center.

record size for CVD laboratory-grown diamond," *GIA Research News*, January 27, 2022).

DiamondView fluorescence imaging showed green and blue colors with a banded pattern. Typical CVD growth striations were clearly visible (figure 11). Green fluorescence was from the H3 defect, produced during HPHT annealing. This banded structure revealed at least eight growth steps to achieve sufficient depth for this large diamond. Additionally, strong blue phosphorescence with similar banding was detected in the DiamondView.

This very large CVD diamond represents a milestone in CVD growth. Mined diamonds with similar size and quality are very rare. We will continue monitoring developments in gem diamond growth technology to ensure all diamonds are properly identified in GIA laboratories.

Ka Wing Tam and Terry "Ping Yu" Poon

CVD Diamonds with Invisible Markings

Laser inscription is a common practice that helps to easily identify a diamond. The inscriptions are so small as to be nearly impossible to read without magnification, but they can be easily read with a loupe or microscope to help match the diamond to a laboratory report. Laser inscription can be done on the girdle, on the center of the table, on a star facet, or under the table surface. Inscriptions under the table surface are very effective from a security standpoint, as they require significant weight loss to remove.

Recently, GIA labs in India tested two diamonds (1.93 and 0.60 ct) with interesting markings. No intentional markings were observed on these samples without magnification, nor could any be seen under a microscope. But when the diamonds were exposed to the deep ultraviolet light of the DiamondView, markings appeared (figure 12). Both samples were CVD laboratory-grown diamonds and

Figure 11. DiamondView imaging of the 34 ct CVD diamond revealed at least eight growth steps.

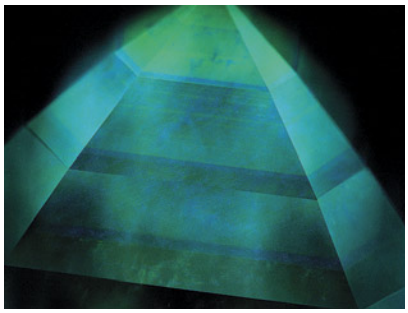

Figure 12. Left: The DiamondView image of the 1.93 ct CVD laboratory-grown diamond shows numbers on the table facet. Right: The 0.60 ct CVD laboratory-grown diamond shows a logo mark on the star facet.

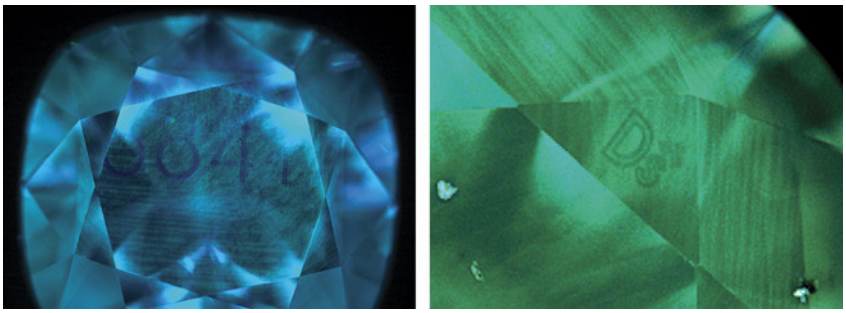

Figure 13. The Lord Hanumana pearl (left, 33.70 × 32.98 × 24.64 mm) and the Lord Ganesha pearl (right, 10.59 × 10.21 × 9.18 mm).

treated with high pressure and high temperature after growth. The invisible markings are thought to be caused by slightly different concentrations of defects, but we do not know how they were created.

The invisible markings in these two diamonds suggest the possible introduction of a new security measure in diamonds, similar to the anti-counterfeiting measure used with passports and banknotes upon exposure to a special light.

Shoko Odake and Priyanka Kadam

PEARLS

Two Pearls of Indian Cultural Significance

In India, pearls (also known as *moti* or *mukta*) and pearl-adorned jewelry have historically been coveted by the affluent and served as symbols of cultural importance for centuries. GIA's Mumbai laboratory has tested various jewelry items set with pearls that were not only artistic in their design but also of great symbolic and religious significance. Two recent submissions consisted of pearls fashioned into the likenesses of Indian deities (figure 13). The first was skillfully crafted to resemble Lord Hanumana, an Indian deity from the epic Ramayana bearing the likeness of a *vanara* (an ancient race of forest-dwellers). The ornament had a total weight of 24.91 g, and its surface was partially drilled in several positions. Yellow metal fittings set with green, white, yellow, and black enamel formed the head, eyes, body, and striped tail. A translucent red stone set on the pearl formed the tongue of the deity (figure 14, left). This baroque pearl was white and light gray in color with orient and measured approximately 33.70 × 32.98 × 24.64 mm. When viewed under 40× magnification, its surface showed typical nacreous structure with overlapping aragonite platelets, and minor surface openings were present on some areas. Most of the surface had good nacre condition, but a few small areas of the nacre were damaged or worn, and remnants of an adhesive glue were visible around some of the decorative enamel inserts.

Energy-dispersive X-ray fluorescence (EDXRF) spectrometry analysis of the pearl showed manganese levels below the detection level of the instrument and a higher strontium content of 1188 ppm. In addition, an inert reaction to X-ray fluorescence (XRF) confirmed saltwater origin. A moderate greenish yellow reaction was observed under long-wave ultraviolet radiation, and a weaker reaction of a similar color was noted under short-wave UV radiation. Such fluorescence reactions in nacreous saltwater pearls are often associated with pearls from the *Pinctada*-species mollusk. Real-time microradiography (RTX) imaging revealed the presence of a very large void that appeared to have been partially filled with a foreign material (figure 14, right). The clearest evidence of the void was observed within the ornament's head as a dark gray area beneath the nacre layer. The outline of this void was consistent with the external shape of the pearl, but the filling material par-

Figure 14. Left: External appearance of the Lord Hanumana pearl. Right: RTX image showing the internal structure. Also indicated are the gemstone tongue, the eyes, the tail, the void, and the filling.

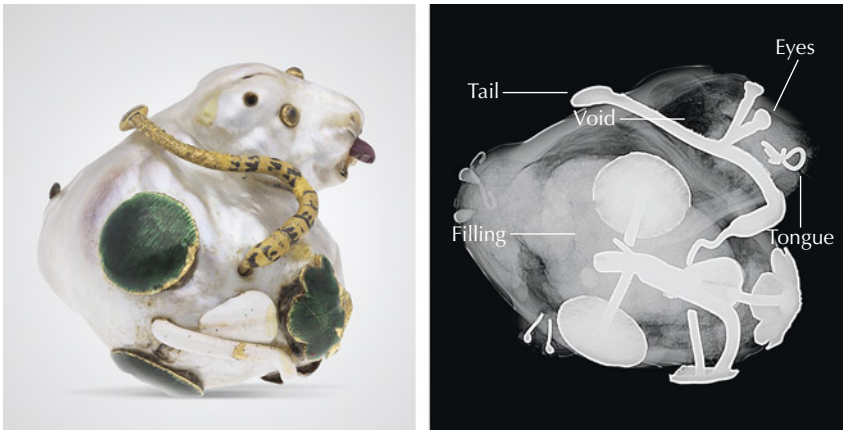

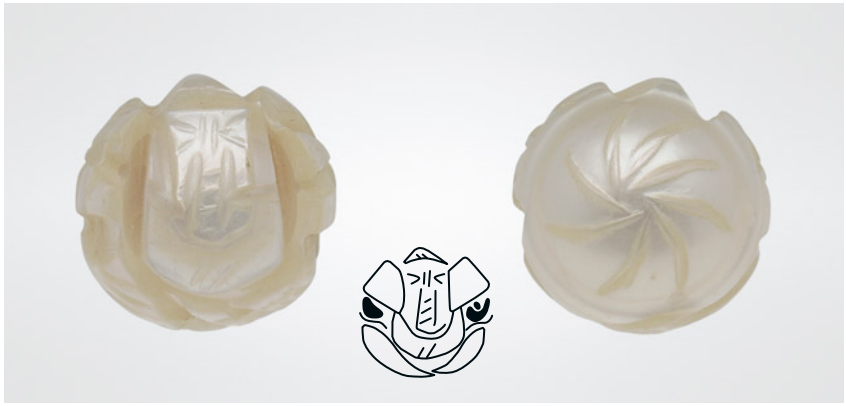

Figure 15. Front view of the Lord Ganesha pearl (left) with a line drawing of features (center) and back view (right).

tially masked the void in RTX and made it harder to see the complete structure clearly. (The radiopaque areas visible on the microradiographs represent the adornments decorating the pearl.) While large voids are more often associated with non-bead cultured pearls, the shape and form of this void resembled those associated with natural pearls. Hollow pearls are often filled (wholly or partially) with a variety of materials including wax, metal, resin, cement, and shell to increase the weight and inflate the perceived value (Winter 2022 Lab Notes, pp. 480–481). In the case of older pearls such as this one, filling can provide enough solid material within the pearl to support all the metal adornments, and it can also improve the durability of the item.

Also submitted was a pearl portraying Lord Ganesha (figure 13, right). The white undrilled, button-shaped pearl weighed 6.27 ct and measured 10.59 × 10.21 × 9.18 mm. Its surface was carefully carved to resemble the Indian deity, with the head of an elephant and the seated body of a man on the front and a swirling pattern on the back (figure 15). EDXRF analysis results showed a high manganese content of 598 ppm and relatively low strontium levels at 376 ppm. These readings were supported by a strong yellowish green fluorescence reaction when exposed to optical XRF (figure 16, left), indicating the pearl was from a freshwater environment. RTX imaging revealed the presence of a small twisted void, along with discoid-like features (figure 16, right) typically seen in non-bead cultured freshwater pearls (K. Scarratt et al., "Characteristics of nuclei in Chinese freshwater cultured pearls," Summer 2000 *G&G*, pp. 98–109).

Figure 16. X-ray fluorescence reaction (left) and an RTX image showing the Lord Ganesha pearl's internal structure (right). A small twisted void and discoid features can be seen in the center.

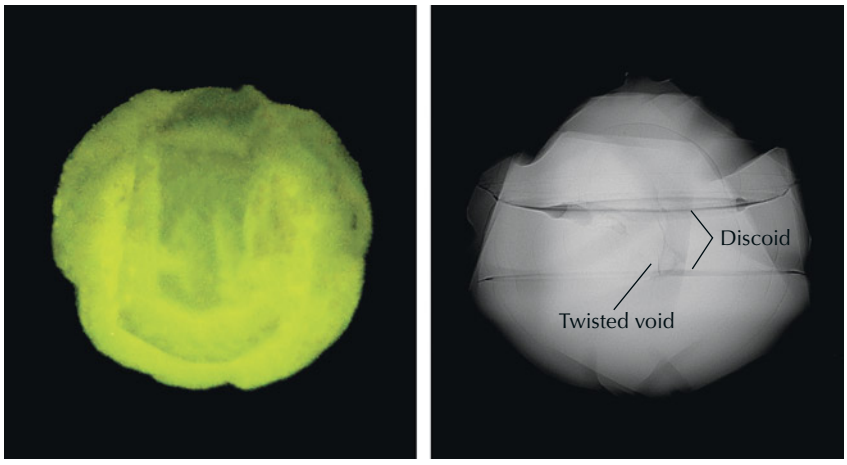

The transformation of pearls into valuable pieces of art is a specialized skill. Indian artists have mastered this ability and can transform pearls into symbolic pieces that have a special connection to ancient Indian scriptures. The laboratory staff at GIA in Mumbai continue to examine intriguing pearls of historical and cultural significance in India.

Nishka Vaz, Rajesh Patel, and Abeer Al-Alawi

A Fascinating Large South Sea Bead Cultured Pearl

A recent noteworthy submission to GIA's Mumbai laboratory contained a loose round, undrilled white pearl with strong orient, weighing 54.96 ct and measuring 19.90 × 19.53 mm (figure 17). Externally the pearl had a smooth, blemish-free surface and exhibited a homogeneous uniform color with a high luster. When viewed under 40× magnification, large and evenly spaced overlapping aragonite platelets were visible which helped account for the silky reflection on the surface. X-ray fluorescence (XRF) analysis gave a relatively inert reaction. Chemical analysis using energy-dispersive X-ray fluorescence spectrometry was performed on two surface areas. The data collected showed manganese levels on both areas below the detection level of the instrument and higher strontium levels of 1162 and 1163 ppm, confirming the pearl formed in a saltwater environment. A moderate greenish yellow reaction was observed under long-wave ultraviolet radiation, and a much weaker greenish yellow reaction was noted under short-wave UV.

Due to the pearl's large size, it was quite intriguing to see the growth

Figure 17. The large round bead cultured pearl weighing 54.96 ct and measuring 19.90 × 19.53 mm.

structure revealed from within. Real-time microradiography (RTX) imaging showed an extremely small bead nucleus together with distinct growth arcs flowing in an even pattern around the nucleus proving it to be a bead cultured (BC) pearl. The exceptional thickness of the nacre growth around the bead was particularly notable (figure 18) (L.M. Otter et al., "A look inside a remarkably large beaded South Sea cultured pearl," Spring 2014 *G&G*, pp. 58–62). The size of the bead and the nacre thickness were measured using an option available on the RTX instrument, resulting in a reading of 6.122 mm for the thickest part of the bead and a range of 5.987 to 6.283 mm, in four different directions, for the overlying nacre. These measurements indicated a composition of more than 96% nacre and less than 4% bead nucleus by volume.

The majority of beads used in the cultivation process of BC pearls are produced from freshwater mollusk shell (*Unionidae*) collected in the United States (A. Homkrajae et al., "Internal structures of known *Pinctada maxima* pearls: Cultured pearls from operated marine mollusks," Fall 2021 *G&G*, pp. 186–205). Due to the high levels of manganese present in freshwater mollusks, such BC pearls would emit a weak or moderate yellowish green fluorescence when subjected to XRF analysis. This reaction is normally based on the size of bead nuclei used in the cultivation process and the thickness of the surrounding nacre. Hence, the reaction observed via XRF for the pearl was relatively weak due to the thickness of its nacre overgrowth (figure 19) (S. Karampelas et al., "Chemical characteristics of freshwater and saltwater natural and cultured pearls from different bivalves," *Minerals*, Vol. 9, No. 6, 2019, article no. 357). Taking all these factors into consideration—external appearance, dimensions, size of the bead nucleus, nacre thickness measurements, and chemistry data—the pearl was classified as a BC pearl produced from the *Pinctada maxima* species.

Over the decades, South Sea BC pearls have played an important part in the global pearl trade. Larger pearls, some more than 20 mm, were also produced, but these are very rare even

Figure 18. RTX images revealing the pearl's internal structure. Left: Diameter of the bead in four directions. Right: The size of the nacre thickness measurements around the bead from its demarcation up to the outer nacre in four directions.

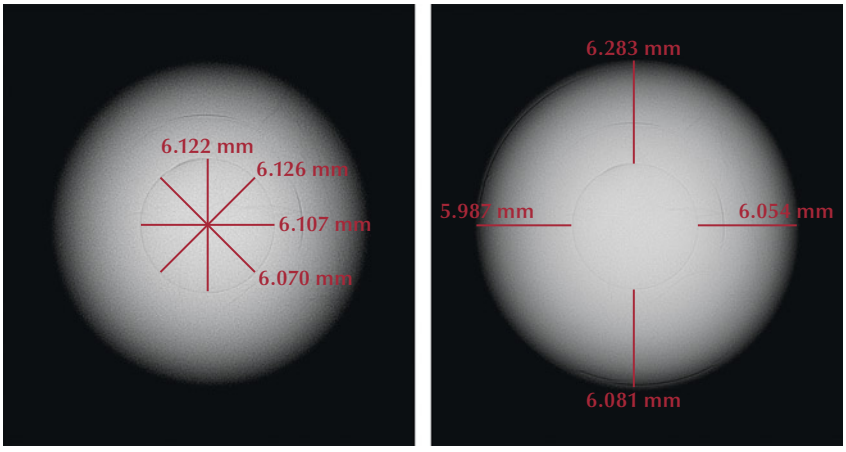

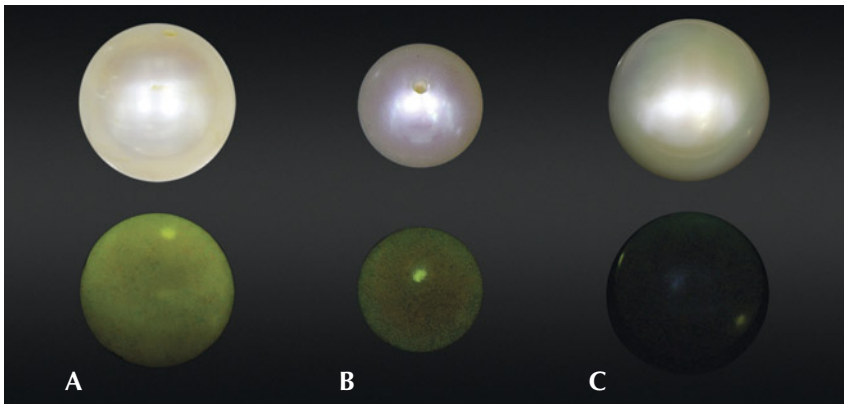

Figure 19. X-ray fluorescence reaction comparison for a freshwater non-bead cultured pearl (A), a saltwater bead cultured pearl with thin to medium nacre thickness (B), and the examined pearl with relatively thick nacre (C).

with today's modern farming methods. Their uniquely large size, silky luster, and greater nacre thickness compared with BC pearls from other mollusks make them more attractive and durable. This has allowed them to establish a prominent position in the cultured pearl value chain as the primary choice of consumers looking for large white to cream, or "golden" BC pearls. As a result, they have been used by renowned jewelry designers in their exclusive collections. GIA continues to test numerous South Sea cultured pearls, and this unique submission to the Mumbai laboratory was particularly notable for its size and fine quality.

Roxane Bhot Jain, Abeer Al-Alawi, and Chunhui Zhou

Fine Linear Structures in Non-Bead Cultured Pearls

Saltwater non-bead cultured (NBC) pearls are defined by the World Jewellery Confederation (CIBJO) as those without an internal bead nucleus that have "formed accidentally or intentionally by human intervention in marine pearl oysters." These are commonly referred to as "keshi" pearls in the trade. GIA's Mumbai laboratory has received many pearl submissions that revealed internal structures typical of NBC pearls such as large voids, elongated linear structures, and some with loose concentric "gaps." However, a recent submission of 23 loose pearls for pearl sorting service proved quite challenging to identify. Externally, all of them looked similar, with a white to light cream color and a medium to high luster. Some possessed a few surface blemishes, but on the whole they were quite clean and appeared cultured.

A majority of the pearls in the lot exhibited concave bases, while a few showed bases with concentric, graduating white to cream-colored rings, with distinct central white frosty patches which were part of the inner subsurface nacreous layers. Four pearls revealing different forms of linear structures were selected from this lot. All were white and button shaped, with sizes ranging from 3.24 × 2.55 mm to 10.33 × 6.84 mm (figure 20). Externally, all their surfaces exhibited typical nacreous overlapping aragonite platelets, with a fingerprint-like pattern when viewed under 40× magnification.

Energy-dispersive X-ray fluorescence spectrometry on the four pearls revealed low manganese levels ranging between 12.60 and 41.10 ppm and high strontium levels between 1767 and 2883 ppm. Additionally, optical X-ray fluorescence analysis yielded an inert reaction, thus confirming their saltwater origin. The pearls showed a moderate bluish green reaction when viewed under long-wave ultraviolet radiation and a weaker bluish green reaction under short-wave ultraviolet radiation. Raman analysis using 514 nm laser excitation showed a doublet at 702 and 705 cm^{-1} and peaks at 1085 and 1463 cm^{-1} indicative of aragonite.

Real-time microradiography (RTX) and X-ray computed microtomography (µ-CT) analysis revealed internal structures that were not straightforward and required more work to reach conclusive results. RTX imaging of pearl 1 showed a prominent, very fine central linear feature horizontal to the base (table 1, row 1). Analysis with µ-CT re-

Figure 20. Four non-bead cultured pearls (samples 1–4, left to right) weighing 0.22 to 4.84 ct.

TABLE 1. Surface appearance and internal structures of four non-bead cultured pearls.

Sample details	Macro image	RTX image	µ-CT image
Pearl 1 0.22 ct 3.24 × 2.55 mm		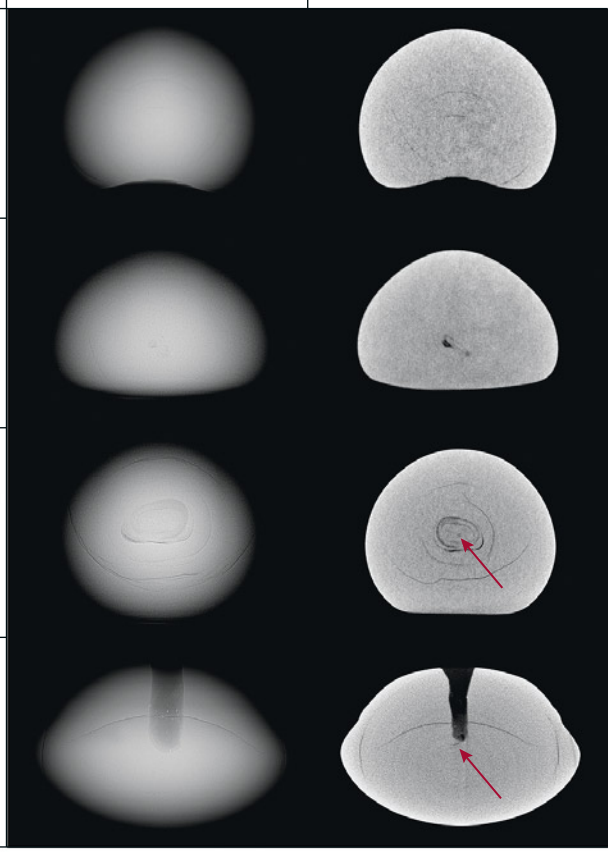	
Pearl 2 0.35 ct 4.10 × 2.81 mm			
Pearl 3[a] 0.81 ct 5.00 × 4.27 mm			
Pearl 4 4.84 ct 10.33 × 6.84 mm			

[a]*The red arrows indicate the identified linear features.*

vealed a more obvious linear feature showing that it was unaligned with the other growth arcs that generally followed the shape of the pearl. This structure was observed in most of the samples in the submitted lot. Externally, a small white frosty central spot was visible on the concave base surrounded by graduating circular rings.

RTX images of pearl 2 revealed a small circular light gray core associated with undefined gray arcs curving along the core in a distorted pattern (table 1, row 2). Moreover, only a couple of weak growth arcs were observed in the outer nacre layers. The structure was very similar to those observed in some natural pearls with small dense cores, making it inconclusive (A. Homkrajae et al., "Internal structures of known *Pinctada maxima* pearls: Cultured pearls from operated marine mollusks," Fall 2021 *G&G*, pp. 186–205). Further µ-CT analysis helped define the main feature, a short and fine linear structure accompanied by a minute void-like feature.

RTX images for pearl 3 revealed a medium-size button-shaped central organic-rich core, which was radiotranslucent and had a thin gray outline (table 1, row 3). This was surrounded by numerous fine growth arcs that followed the shape of the core. Although this organic-rich core looked quite natural from the RTX images, µ-CT images revealed a short linear feature in the center of the core, suggesting an NBC pearl.

The largest sample, pearl 4, had been partially drilled, and the drill hole was quite large (table 1, row 4). It was unlike the thinner and shorter drill holes often used for weight retention in natural pearls. While the choice of drill hole thickness is not decisive evidence on its own, it may be a useful indicator (Spring 1986 Lab Notes, pp. 51–52; Summer 1986 Lab Notes, p. 111). Externally, the pearl had a rounded base and a circled circumference with multiple deep indentations associated with the circled grooves. The RTX images showed minute metal remnants (visible as radiopaque white specks) within the drill hole and extensive curved growth arcs throughout the pearl, with additional arcs located on adjacent boundaries. The pearl showed minimal tight growth structure, and its external appearance aroused suspicion. Further examination via µ-CT analysis revealed a small linear feature that had been partially removed by the drilling.

Reaching a conclusion would be very challenging, if not impossible, using RTX analysis alone.

Given the volume of button-shaped pearls the Mumbai laboratory has been testing, it is quite evident that large quantities of such pearls are circulating in the market. These pearls mostly have smooth surfaces and high untreated luster. The linear features could not be identified in all the pearls using RTX alone due to a number of factors including size, appearance, radiotranslucency, and orientation. It is not difficult to remove minute linear structures by drilling, and such pearls could easily be passed off as natural due to the presence of fine growth features around the center. But with the availability of advanced technology, especially μ-CT imaging, remnants of the linear structure were evident in certain orientations. In some cases, with the proper alignment of the drill hole, such small linear structures may also be visible in the RTX images. This requires considerable skill and patience to align, starting from the thickest direction first with respect to the shape of the pearl and then repositioning the same pearl 90° in the profile view. Therefore, it may be risky to rely on RTX results alone (S. Karampelas et al., "X-ray computed microtomography applied to pearls: Methodology, advantages, and limitations," Summer 2010 *G&G*, pp. 122–127).

By analyzing these challenging internal structures using modern equipment, GIA and other laboratories aim to protect consumers by creating awareness of them and minimizing the chances of misidentification.

Gauri Sarvankar, Abeer Al-Alawi, Karan Rajguru, and Roxane Bhot Jain

Figure 21. An imitation emerald in the form of a chess knight measuring approximately 35.05 mm in height.

Figure 23. An assemblage of plastic and various minerals imitating rough emerald in matrix, measuring approximately 51.79 mm in height.

PLASTIC Imitations of Emerald

GIA's New York laboratory recently examined two imitations, each submitted for an emerald identification report, that might have been convincing to the untrained eye. One was a chess piece weighing 46.55 ct (figure 21). At a glance, the knight appeared to be carved emerald with remnants of metallic yellow "matrix" still intact. However, the low heft and relatively warm feel of the piece suggested otherwise. Microscopic examination revealed an aggregate structure composed of jagged blocks, clearly illustrated under long-wave ultraviolet light due to its marked whitish fluorescence, typical of plastic (figure 22). The presence of gas bubbles and bluish dye concentrations indicated that the material was in fact an assemblage. The lack of a polished surface prevented a refractive index reading. Infrared and Raman spectroscopy were used to identify the main component as plastic; no beryl was detected. The metallic yellow crystal fragments were identified as pyrite, consistent with matrix associated with natural emeralds, notably those from Colombia.

The second imitation emerald (figure 23) was in the form of an elongated hexagonal "rough" emerald crystal embedded in a "matrix" of white and metallic yellow crystals, with a total weight of 179.71 ct. It too appeared natural to the unaided eye, but microscopic examination quickly distinguished the specimen as an imitation.

Figure 22. A closer look at the knight's head (left, in daylight) reveals the material's aggregate structure when viewed under long-wave ultraviolet light (right).

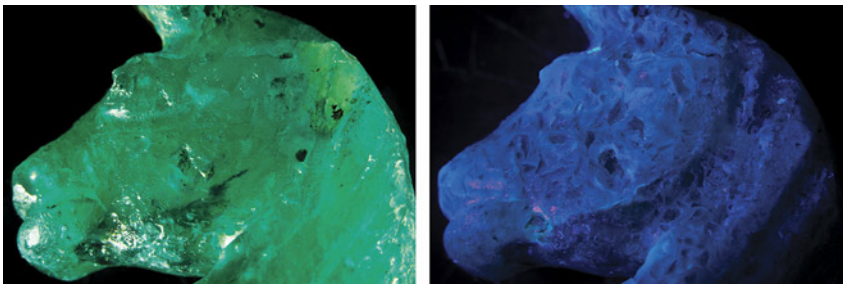

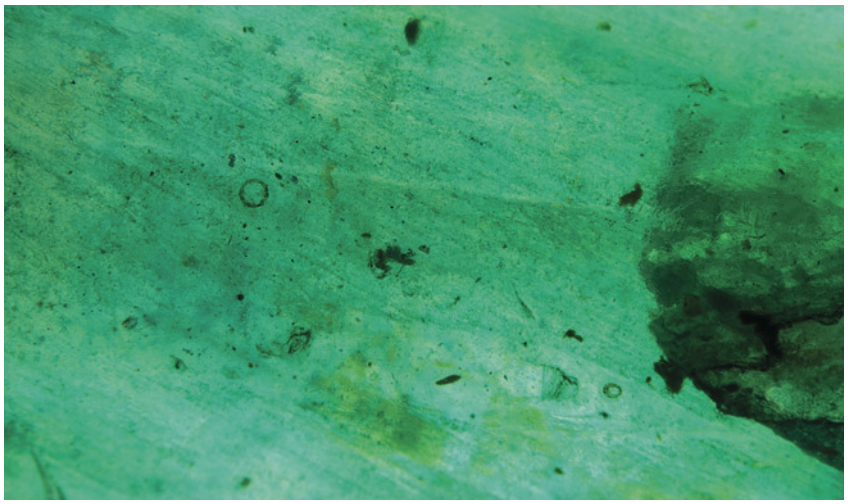

Figure 24. Gas bubbles and bluish green dye concentrations indicate that this "crystal" is in fact a manufactured product. Field of view 8.23 mm.

Figure 25. An exceptional pink zektzerite, cut as a square modified step cut, measuring 8.08 × 7.39 × 6.89 mm and weighing 2.95 ct.

The "emerald" portion of the rough contained large gas bubbles as well as bluish green dye concentrations (figure 24), an overall blotchy color appearance, and parallel surface striations. This material was identified as plastic using Raman and infrared spectroscopy. The surface striations were presumably created in the mold or carved to resemble the texture of a rough emerald crystal. Raman spectroscopy revealed that the smaller crystals mixed into the plastic were quartz and beryl. The white portion of the "matrix" was identified as calcite and the metallic crystals as pyrite, making this piece another convincing imitation of Colombian emerald.

The natural materials incorporated into these mostly plastic manufactured products might lead some astray upon first inspection. These two pieces demonstrate the need for a deeper inspection of all materials, regardless of how genuine they may seem on the surface.

Emily Jones and Abadie Ludlam

Pink ZEKTZERITE

Zektzerite, a member of the tuhualite group, is a very rare collectible mineral currently mined from only two sources: Okanogan County in the U.S. state of Washington (Spring 2011 Gem News International, p. 61), and the Darai-Pioz Valley in Tajikistan (L.A. Pautovet et al., "Zektzerite—occurrence in Tadzhikistan," *Mineralogicheskii Zhurnal*, Vol. 14, pp. 75–78). With the chemical formula $NaLiZrSi_6O_{15}$, these rare crystals are found in miarolitic cavities in riebeckite granite, along with many other rare minerals. The zektzerite crystals found in these locations are primarily between 4 mm and 15 mm and usually yield small faceted gems weighing less than 2 ct. This material is typically found with a low transparency and muted color saturations. Perfect cleavage in two directions and a brittle tendency make this fragile stone very difficult and risky to cut. Due to its low durability and overall dull appearance, collectors tend to leave zektzerite in its natural rough state.

An outstanding example of faceted gem-quality zektzerite (figure 25) was recently submitted to GIA's Carlsbad laboratory. The stone weighed 2.95 ct, measured 8.08 × 7.39 × 6.89 mm, and had a refractive index ranging between 1.578 and 1.584. A specific gravity of 2.81, along with Raman and infrared spectroscopic testing, all matched zektzerite, with no indication of dye or polymers. The outstanding pink color, relatively high clarity, and impressive size of this stone sets this specimen far above any other faceted zektzerite previously reported.

Jamie Price

PHOTO CREDITS
Towfiq Ahmed—1; Jessa Rizzo—2; Annie Haynes—3; Jemini Sawant—4, 12; Shiva Sohrabi—5; Johnny (Chak Wan) Leung—6, 8; Tsz Ying Fong—7; Ka Wing Tam—9, 11; Gaurav Bera—13, 14 (left), 15, 17, 19, 20; Kristin Reinheimer—21; Emily Jones—22; Michele Wong—23; Abadie Ludlam—24; Diego Sanchez—25